# Photo-modulated regeneration of hypercrosslinked polymer adsorbents for water treatment

Separation and Purification Technology 329 (2024) 125142

Contents lists available at ScienceDirect

Separation and Purification Technology

journal homepage: www.elsevier.com/locate/seppur

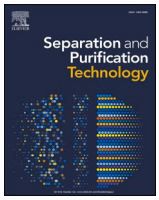

# Photo-modulated regeneration of hypercrosslinked polymer adsorbents for water treatment

Aotian Liu [a], Xiuming Wei [a], Shiliang Lin [a], Liang Ding [a], Yi Huang [a], Xianfeng Fan [a], Pei Li [b,*], Cher Hon Lau [a,*]

[a] School of Engineering, The University of Edinburgh, Robert Stevenson Road, Edinburgh EH9 3BF, UK
[b] School of Material Science and Engineering, Beijing University of Chemical Technology, Chaoyang District, Beijing 100029, PR China

ARTICLE INFO

*Keywords:*
Hypercross-linked polymers
Dyes
Desorption
Photosensitive
Isotherm model
Kinetics

ABSTRACT

Hypercrosslinked polymers (HCPs) are highly effective adsorbents for removing dyes from water. However, the regeneration of such adsorbents is typically achieved with energy-intensive thermal methods or with solvents that generate chemical waste. Here in this proof of concept study, we used HCPs loaded with azobenzene molecules (HCPs@Azo) that were developed in our previous work, and four types of dyes – Methyl Orange (MO), Methylene Blue (MB), Rhodamine B (RB), Uniblue A (UA), at concentrations ranging from 10 to 500 mg $L^{-1}$, to demonstrate the feasibility of photo-modulated regeneration of HCP-based adsorbents. Azobenzene in HCP pores reduced dye adsorption by 4–31 %, but upon photo-isomerisation from *trans* to *cis* states, led to the desorption of 1.7–20 % dyes that were previously adsorbed. These desorption capacities were 71–209 % higher than using water for regeneration. Compared to the traditional method using organic solvents such as methanol to regenerate HCP-based adsorbents, our approach of photo-modulated regeneration led to the desorption of 50 % more MO and MB dyes. HCPs@Azo also demonstrated good reusability, showing comparable photo-modulated adsorption and desorption capacities after four cycles of UV–visible light irradiation. Results from this work can potentially pave the way for solvent-less regeneration of adsorbents, creating a waste-less adsorbent regeneration process.

## 1. Introduction

About 1.6 million tons of synthetic dyes are produced annually [1] and applied in different industries including food, textile, cosmetics, printing, pigment, and paint [2], and 10–15 % of these dyes are discharged into our living environment [3]. This form of pollution can be mitigated by adsorption where dyes are removed as the solid phase from water [4] where adsorbates (in this case, dyes) accumulate at the adsorbent surface [5]. Physical adsorption depends on Van der Waals forces interaction [6,7], while chemical adsorption forms chemical bonds between adsorbents and adsorbates. Advantages of adsorption include its simplicity in deployment, lower cost, and ease of recycling [8]. Examples of such adsorbents include activated carbon [9,10], zeolites [11,12], metal–organic frameworks (MOFs) [13,14], graphene oxide [15,16], hyper-crosslinked polymers (HCPs) [17].

The use of adsorbents in water treatment is a well-established process due to their excellent efficacy in removing dyes from water. For example, activated carbon adsorbed 321 mg $g^{-1}$ of Methylene Blue from 100 mg $L^{-1}$ solution [10]. Only 25 mg of metal–organic frameworks were required to adsorb 95 % of Methylene Blue dyes from a 5 mg $L^{-1}$ aqueous solution [14]. 10 mg of graphene oxide adsorbed 99 % of Methylene Blue from water after 2 min [15] while 10 mg of HCPs adsorbed 100 mg of RB in 1 L of water within 10 min [17]. Despite excellent adsorption capacities, the main limitation of these adsorbents lies in desorption where this process is mandatory for regeneration or releasing the captured dye molecules.

In desorption, adsorbates are displaced from the adsorbent surface by replacement with solvent molecules (solvent regeneration) [18,19] or by tailoring the surface energy to affect adsorption (thermal regeneration) [2]. Solvent regeneration creates significant waste while thermal methods consume large amounts of energy. For example, thermal regeneration of sludge-based activated carbon is achieved at 300 °C for 30 min, desorbing 93% of adsorbed Methylene Blue [20]. Acid/alcohol mixtures are required to desorb 84–95 % of Methylene Blue dyes from

* Corresponding authors.
*E-mail addresses:* lipei@buct.edu.cn (P. Li), cherhon.lau@ed.ac.uk (C.H. Lau).

https://doi.org/10.1016/j.seppur.2023.125142
Received 28 July 2023; Received in revised form 4 September 2023; Accepted 18 September 2023
Available online 22 September 2023

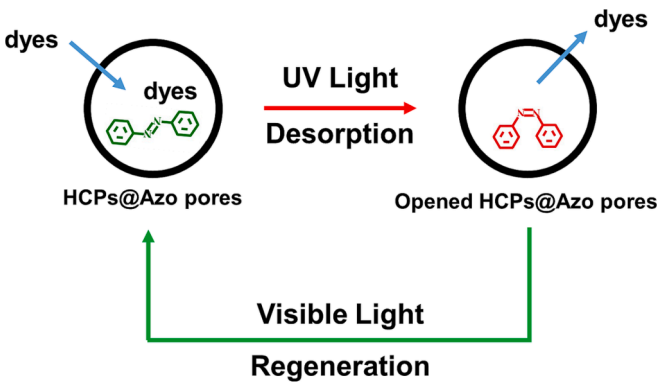


**Fig. 1.** Cyclic dye adsorption and desorption process of photosensitive adsorbent. HCPs@Azo. (i) *trans*-HCPs@Azo adsorbed various dyes (MO, MB, RB and UA) from water. (ii) *trans–cis* isomerisation of azobenzene upon UV irradiation led to the desorption of dyes. (iii) Regeneration of HCPs@Azo for subsequent re-use is achieved by visible light irradiation.

metal-organic frameworks [21,22]. Clearly, a regeneration mechanism that does not generate solvent waste and consumes significant energy is required for adsorption to align with the expectations of a net-zero, zero-avoidable waste economy.

This can be potentially achieved with light-controlled mechanisms where light-controlled desorption can reduce energy consumption by >90 %, and obviate the generation of chemical waste associated with desorption [26], where silica nanoparticles [23,24] and $Bi_2O_2CO_3$ nanosheets [25] loaded with photo-switches such as azobenzene show light-controlled dye desorption capacities of 100% for Brilliant Blue, 90 % for Rhodamine B and 79 % for Methylene Blue. In the case of mesoporous silica decorated with azobenzene molecules that functioned as light-controllable gates,[23] 60 % of the dyes were desorbed in the presence of ethanol without any for photo-irradiation, while the remaining 40 % of dyes were desorbed only after UV irradiation. The main desorption mechanism in these light-responsive mesoporous silica still relied on solvent displacement while light-controlled desorption is exploited to ensure complete dye desorption. Nonetheless, these works show that desorption can be improved *via* photo-modulation by triggering structural changes in adsorbents [23,24] or altering coordination between dye molecules and adsorbent surface [25]. To date, there is no HCP based material that relies solely on light-controlled mechanisms to control both adsorption and desorption.

Here we hypothesize that desorption of dyes from HCPs can be achieved with light-controlled reversible pore size changes observed in our previous work where we developed photo-responsive HCPs (HCPs@Azo) comprising 8.9 wt% of azobenzene within their micropores [27]. Photo-isomerisation of azobenzene from *trans* to *cis* states is accompanied by a dimension change, from 5.5 Å (*cis*) to 9 Å (*trans*) [28-30]. This photo-reversible size change in azobenzene increased accessible HCP pore sizes, from 10 Å to 14 Å and volume, from 0.832 $cm^3\ g^{-1}$ to 1.009 $cm^3\ g^{-1}$.

Rather than utilizing the *cis*-to-*trans* isomerization of azobenzene to benefit adsorption for $CO_2$ as shown in our previous work [27], here we exploited the *trans*-to-*cis* isomerization of azobenzene to trigger and control dye desorption from HCP pores as a function of photo-modulated pore size changes (Fig. 1). In our approach, *trans*-HCPs@Azo was deployed to adsorb 10–500 mg $L^{-1}$ of Methyl orange (MO), Methylene Blue (MB), Rhodamine B (RB), and Uniblue A (UA) from aqueous solutions. Upon UV irradiation of dye-loaded HCPs@Azo, *trans*-azobenzene was isomerized into the *cis* state, leading to the desorption of 1.7–20% of MO, MB, RB, and UA dyes in water. Here it is important to highlight that the role of water i.e., solvent is not for driving desorption, as per literature,[23,24] but for dissolution of dyes. These photo-modulated desorption capacities were 71–209 % higher than water regeneration without UV stimuli. Our approach of photo-modulated desorption released 50 % more MO and MB dyes than solvent desorption. Photo-modulated dye adsorption and desorption capacities of HCPs@Azo were maintained after cyclic testing, indicating good regeneration ability. The main advantages of our approach include obviating waste generation and significant energy consumption that are associated with traditional solvent- and thermal-based approaches.

## 2. Experimental

### 2.1. Materials

Waste Styrofoam was collected from discarded solvent packaging supplies at the University of Edinburgh. Iron chloride (98 %, $FeCl_3$) and 1,2-dichloroethane (DCE) were purchased from Alfa Aesar. Azobenzene, Methylene blue (MB), Methyl Orange (MO), Rhodamine B (RB), Uniblue A (UA), and formaldehyde dimethyl acetal (98 %, FDA) were purchased from Sigma-Aldrich. Ethanol (≥99.8 %), methanol (≥99.9 %), chloroform (≥99.8 %), and acetone were obtained from Fisher Chemical. All chemicals and solvents were used directly without any purification.

### 2.2. Preparation of hypercross-linked polymers (HCPs)

Referring to the work of Lau and co-workers [17], here we synthesized HCPs using a mass ratio of 1:5:5 between Styrofoam, $FeCl_3$ (catalyst), and FDA (crosslinker). Briefly, 50 mL DCE and 5 g FDA were added into a 100 mL two-neck round-bottom flask to dissolve 1 g waste Styrofoam and mix with 5 g $FeCl_3$. The mixture was refluxed for 24 h at 80 °C at a stirring speed of 270 rpm. The product was collected and washed with chloroform, methanol, acetone, and water. The washed product was dried in a vacuum oven for 12 h at 120 °C to obtain brown powders.

### 2.3. Preparation of HCPs@Azo

Following the protocols of Liu *et al.* [27] and Müller *et al.*[31], we added 200 mg HCPs into a 25 mg $mL^{-1}$ ethanolic solution of azobenzene and allowed this mixture to rest for 12 h to optimise azobenzene content in HCPs. Figure S4 shows how azobenzene content in HCPs varied over different immersion durations. The product was retrieved by filtration, washed with ethanol for 10 s, and dried at 25 °C for 24 h to obtain HCPs@Azo.

### 2.4. Material characterization

Elemental analysis (EA) was performed to analyze the content of different elements (C, N, H, and O) in HCPs@Azo, using a Thermo Fisher Scientific Flash SMART 2000 setup. The furnace temperature was set at 950 °C. The flow rate of helium as carrier gas was 140 mL $min^{-1}$ and the total run time was 660 s. A thermal Conductivity Detector (TCD) was used as the instrument detector.

X-ray photoelectron spectroscopy (XPS) was carried out using a Kratos Axis SUPRA XPS. All data was recorded at a spot size of 700 × 300 μm with a voltage of 150 W, a pressure below $10^{-8}$ Torr, and 294 K room temperature. The pass energy of survey scans was 160 eV, the pass energy of high-resolution scans was 20 eV, the filament current was 0.27 A, the charge balance was 3.3 V, and filament bias was 3.8 V. A monochromated Al kkα X-ray source (1486.7 eV), a spherical sector analyzer, 3 multi-channel resistive plate and 128 channel delay line detectors were used in the measurements.

Water contact angle (WCA) measurements were obtained from a ramé-hart goniometer (model-250). A water drop was dripped from a 22-gauge needle. The WCA images were captured within 1 min.

Fourier transform infrared spectroscopy (FTIR) was measured with an ATR-FTIR (Nicolet iS10 with Smart iTX Diamond accessory, Thermo Fisher Scientific, Waltham, MA) with a resolution of 0.48 $cm^{-1}$ from

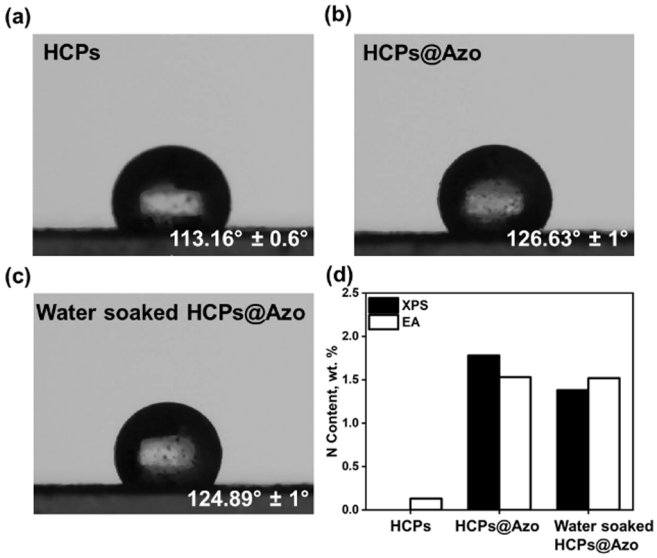


**Fig. 2.** The water contact angle (WCA) of (a) HCPs are increased by 12% upon (b) incorporation of azobenzene into HCP pores (HCP@Azo). (c) Unchanged WCA of water-soaked HCP@Azo indicated that water did not displace azobenzene molecules present in the pores of HCPs@Azo. (d) A comparison of XPS and elemental analyses (EA) of N % mass content in HCPs@Azo, before and after water immersion.

4000 $cm^{-1}$ to 500 $cm^{-1}$ at 64 scans to observe the chemical structural change of adsorbents.

Scanning electron microscopy (SEM) micrographs were captured on ZEISS Crossbeam 550 FIB-SEM. The samples were coated with 20 nm layer of gold by sputtering before loading on the sample holders.

### 2.5. Adsorption experiments

10 mg HCPs and visible-light-pretreated *trans*-HCPs@Azo (visible light: ZLUV LAMP 450 nm, power: 6 W) were added into 10 mL of aqueous solutions containing MB, MO, RB, UA, with different initial dye concentrations (10 mg $L^{-1}$, 30 mg $L^{-1}$, 50 mg $L^{-1}$, 70 mg $L^{-1}$, 100 mg $L^{-1}$, 200 mg $L^{-1}$, 300 mg $L^{-1}$, 400 mg $L^{-1}$, 500 mg $L^{-1}$, 600 mg $L^{-1}$ (only RB), 700 mg $L^{-1}$ (only RB)). These mixtures were stirred with a magnetic stirrer at 200 rpm at 25 °C for 24 h to achieve equilibrium.

After adsorption, the mixed suspensions were centrifuged at 12000 rpm for 30 min in a high-speed centrifuge (ALC PK 131R Multi-Speed Refrigerated Centrifuge). The supernatants were collected and diluted. Dye content in the diluted supernatants was determined with an Evolution 60 UV–visible spectrophotometer. The concentration of residual dyes in solution was calibrated and computed by the Beer-Lambert law [32] at the optimum absorbance wavelength of 664, 464, 554, and 596 nm for MB, MO, RB, and UA, respectively, in the 300–800 nm absorbance range (Figure S13). The adsorption capacity ($q_e$, mg $g^{-1}$) and the efficiency of adsorption (η, %) at equilibrium were calculated using the following equations:

$$q_e = (C_0 - C_e) \times \frac{V}{m} \quad (1)$$

$$\eta\% = \frac{C_0 - C_e}{C_0} \times 100 \quad (2)$$

where V is the volume of dye solution (L), m is the mass of adsorbent (HCPs, *trans*-HCPs@Azo, g), $C_0$ is the initial concentration of dyes (mg $L^{-1}$), $C_e$ is the concentration of residual dyes at equilibrium after adsorbing by adsorbents (mg $L^{-1}$). Adsorbents containing the dyes were collected (*via* filtration), dried in the oven at 100 °C for 2 h, and used for desorption studies. For further kinetic studies, 10 mg of adsorbents were added to a 10 mL solution comprising a dye concentration of 100 mg $L^{-1}$ (similar to those from dye houses [33]). The mixtures were stirred at 200 rpm at 25 °C for 2, 4, 6, 8, 10, 15, 20, 30, 40, 80, 120, 160, 200, and 240 min. The supernatants were collected after centrifugation, diluted, and determined by UV–Vis spectrophotometry.

### 2.6. Desorption experiments

Control experiments demonstrating effects of water regeneration were perfomed by adding HCPs and *trans*-HCPs@Azo into beakers containing 10 mL of deionized water and stood for 4 h to achieve equilibrium. These adsorbents were not UV-irradiated.

In another set of experiments, dye-loaded HCPs and HCPs@Azo were first irradiated with UV light (UV light: ZLUV LAMP 365 nm, power: 6 W) for 30 min prior immersion in water. Once in water, these adsorbents were also irradiated with UV light for 30 min and stood for 4 h. A UV-irradiation time of 30 min was chosen here based on published protocols [23,31,34,35]. Adsorbents in these experiments were named as HCPs-UV and *cis*-HCPs@Azo-UV, respectively.

Supernatants from these four experiments were collected, diluted, and characterized using a UV–Vis spectrophotometer. The desorption capacity of adsorbents ($q_{De}$, mg $g^{-1}$) and the efficiency of desorption ($\eta_D$, %) at equilibrium were calculated with the following equations:

$$q_{De} = C_{De} \times \frac{V}{m} \quad (3)$$

$$\eta_D\% = \frac{q_{De}}{q_e} \times 100 \quad (4)$$

where V is the volume of deionized water (L), m is the weight of dyed adsorbents (g), $C_{De}$ is the concentration of dyes in deionized water (mg $L^{-1}$), $q_e$ is the adsorption capacity of adsorbents (mg $g^{-1}$).

Desorption kinetics of HCPs, *trans*-HCPs@Azo, HCPs-UV, and *cis*-HCPs@Azo-UV were determined using samples that were used to adsorb dyes from 100 mg $L^{-1}$ mixture. These adsorbents were weighed before discharging them into deionized water. Adsorbents were retrieved from these solutions after 2, 5, 10, 20, 30, 40, 80, 120, and 160 min. During desorption experiments, HCPs-UV and *cis*-HCPs@Azo-UV samples were continuously irradiated with 365 nm UV light for 4 h. After desorption, the supernatants were collected, diluted, and characterized using the UV–Vis spectrophotometer.

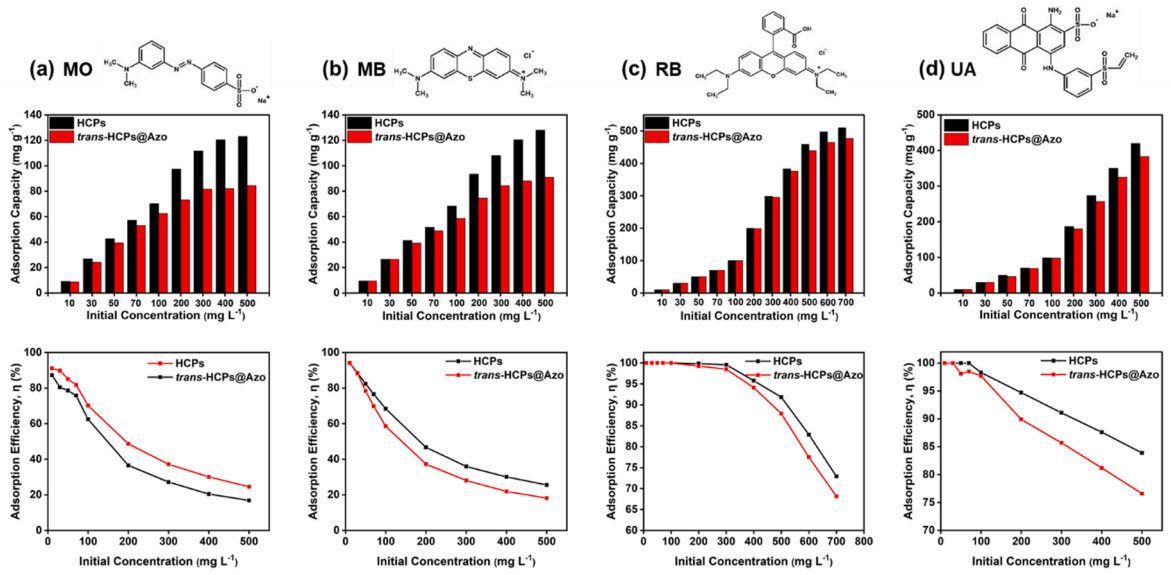


**Fig. 3.** Adsorption capacities and efficiencies of HCPs (black) and *trans*-HCPs@Azo (red) for (a) MO, (b) MB, (c) RB and (d) UA of the initial concentration from 10 mg $L^{-1}$ to 500 mg $L^{-1}$ (700 mg $L^{-1}$ for RB only). (For interpretation of the references to color in this figure legend, the reader is referred to the web version of this article.)

### 2.7. Reusability experiments

10 mg *trans*-HCPs@Azo was immersed in 10 mL of solutions comprising 10 mg $L^{-1}$ of dyes (the lowest concentration discharged from dye houses [33]). The mixture was allowed to stand for 24 h. The amount of residual dye content in the supernatant was characterized using a UV–vis spectrophotometer. The dye-containing *trans*-HCPs@Azo adsorbents were collected by filtration and dried in an oven at 100 °C for 2 h. The dried *trans*-HCPs@Azo was irradiated with UV light for 30 min before immersion in water, yielding *cis*-HCPs@Azo-UV samples. *Cis*-HCPs@Azo-UV samples were then added into 10 mL of deionized water. These samples were continuously irradiated with UV light for 1 h throughout the desorption experiment. The supernatant was collected, and the dye concentration of this solution was determined by UV–Vis spectrophotometry. *cis*-HCPs@Azo-UV was collected after desorption, dried, and irradiated with visible light for 1 h to revert to *trans*-HCPs@Azo. The regenerated *trans*-HCPs@Azo was added into 10 mL of solutions comprising 10 mg $L^{-1}$ of dyes to repeat the above processes for three times.

## 3. Theory

### 3.1. Isotherm models

To describe the solid–liquid adsorption and desorption process, the most widely used isotherm models are the Langmuir model [36] and the Freundlich model [37]. The Langmuir isotherm model assumes that monolayer adsorption or desorption occurs on the homogeneous surface of adsorbents and there is no interaction between adsorbed dye molecules and the neighboring active sites [20]. Langmuir model is calculated by:

$$q_e = \frac{q_{max} K_L C_e}{(1 + K_L C_e)} \tag{5}$$

$$q_{Dmax} = q_{\max(adsorption)} - q_{\max(desorption)} \tag{6}$$

where $q_{max}$ is the maximum amount of dyes in adsorbents (mg $g^{-1}$), $q_{Dmax}$ is the maximum desorption capacity of adsorbents (mg $g^{-1}$), $q_e$ is the amount of dyes in the adsorbents at equilibrium (mg $g^{-1}$), $C_e$ is the concentration of dyes in solution at equilibrium (mg $L^{-1}$), $K_L$ is the Langmuir constant related to the energy of adsorption or desorption (L/mg). To get $q_{max}$ and $K_L$, equation (5) can be transformed into the following linear equation:

$$\frac{C_e}{q_e} = \frac{C_e}{q_{max}} + \frac{1}{K_L q_{max}} \tag{7}$$

The Freundlich isotherm model describes the multilayer adsorption or desorption on a heterogeneous surface [38] with the interaction of adsorbed molecules and non-equivalent energy active centers [39]. The Freundlich model can be represented as:

$$q_e = K_F \times C_e^{\frac{1}{n}} \tag{8}$$

where $q_e$ is the amount of dyes in the solid phase at equilibrium (mg $g^{-1}$), $C_e$ is the concentration of residual (adsorption) or desorbed (desorption) dyes in solution at equilibrium (mg $L^{-1}$), $K_F$ is the Freundlich isotherm constant [(mg/g)(L/mg)$^{1/n}$], n is the characteristic constant about adsorption or desorption intensity. Equation (8) can be linearized by taking natural logarithm to:

$$lnq_e = lnK_F + \frac{1}{n} lnC_e \tag{9}$$

### 3.2. Kinetic models

To study the kinetics of the adsorption and desorption process, Pseudo-first-order and Pseudo-second-order [40-42] models are commonly fitted using experimental data. The Pseudo-first-order model assumes that adsorption and desorption rate depend on the concentration of dyes and the amount of remaining dyes on the adsorbent surface [43,44]. The equation is given as:

$$q_t = q_e\left(1 - e^{-k_1 t}\right) \tag{10}$$

where $q_t$ is the amount of dyes adsorbed or desorbed (mg $g^{-1}$) at a given time t (min), $q_e$ is the dyes adsorption or desorption capacity of adsorbents (mg $g^{-1}$) at equilibrium, $k_1$ is the rate constant of Pseudo-first order-model (1/min). By natural logarithm transformation, equation (10) becomes:

$$\ln(q_e - q_t) = \ln q_e - k_1 t \tag{11}$$

The Pseudo-second-order kinetic order model states the speed of adsorption and desorption depend on the adsorption and desorption ability of adsorbents [45]. The equation is shown below:

**Table 1**
The parameters of Langmuir and Freundlich isotherm models for MO, MB, RB and UA adsorbed onto HCPs and *trans*-HCPs@Azo.

| Isotherm models | Parameters | MO | MB | RB | UA |
|---|---|---|---|---|---|
| Langmuir (HCPs) | $q_{max}$ (mg $g^{-1}$) | 126.9 | 130.7 | 510.2 | 406.5 |
| | $K_L$ (L/mg) | 0.056 | 0.043 | 0.825 | 0.248 |
| | $R^2$ | 0.997 | 0.990 | 0.999 | 0.954 |
| Freudlich (HCPs) | $K_F$ [(mg/g)(L/mg)$^{1/n}$] | 15.63 | 15.29 | 258.9 | 78.99 |
| | n | 2.6 | 2.61 | 7.1 | 2.64 |
| | $R^2$ | 0.9 | 0.962 | 0.953 | 0.998 |
| Langmuir (*trans*-HCPs@Azo) | $q_{max}$ (mg $g^{-1}$) | 86.5 | 92.9 | 476.2 | 377.4 |
| | $K_L$ (L/mg) | 0.071 | 0.06 | 0.592 | 0.127 |
| | $R^2$ | 0.999 | 0.997 | 0.999 | 0.953 |
| Freudlich (*trans*-HCPs@Azo) | $K_F$ [(mg/g)(L/mg)$^{1/n}$] | 13.19 | 15.29 | 208.6 | 59.48 |
| | n | 2.87 | 3.08 | 5.96 | 2.56 |
| | $R^2$ | 0.834 | 0.938 | 0.922 | 0.968 |

$$q_t = \frac{q_e^2 k_2 t}{1 + q_e k_2 t} \tag{12}$$

where $q_t$ and $q_e$ are the amount of adsorbed or desorbed dyes (mg $g^{-1}$) at any time t (min) and equilibrium, respectively. $k_2$ is the rate constant of the Pseudo-second-order model (g/mg·min). Equation (12) can be changed to a linear form:

$$\frac{t}{q_t} = \frac{1}{k_2 q_e^2} + \frac{t}{q_e} \tag{13}$$

## 4. Results and discussion

### 4.1. Material properties

HCPs and HCPs@Azo synthesized according to our previously published protocol [27] were used in this study for dye adsorption and desorption. The increased N content and decreased contents of C, H and O elements demonstrated that the azobenzene guest molecules had successfully incorporated into the HCPs@Azo structures (Table S2). The photo-responses of HCPs@Azo were determined using UV–Vis spectroscopy (Figure S1) where we observed that the absorption intensities of HCPs@Azo at 320 nm (π–π*) and 450 nm (n–π*) changed reversibly upon UV and visible light irradiation [31]. Due to the presence of photosensitive guest azobezene molecules in HCP pores, the Brunauer Emmett Teller (BET) surface area, pore volume and pore size distribution of HCPs@Azo pores were photo-modulated with different light wavelengths (Figure S2, Table S1).

With UV irradiation (365 nm), the physical dimensions of azobenzene molecules were reduced from 9 Å to 5.5 Å. This *trans-to-cis* isomerization of azobenzene within HCP micropores enhanced the accessible BET surface area and pore volume to 1024 $m^2 g^{-1}$ and 1.009 $cm^3 g^{-1}$, respectively. As *cis*-azobenzene reverted to the *trans* state upon vis-irradiation (450 nm), the BET surface area and pore volume of *trans*-HCPs@Azo were reduced to 862 $m^2 g^{-1}$ and 0.832 $cm^3 g^{-1}$, respectively.

Water contact angle (WCA) measurements showed that physical steeping of azobenzene also impacted the hydrophobicity of HCPs (Fig. 2). WCAs larger than 90° indicated hydrophobic adsorbents that are ideal for removing dyes from aqueous environments [46]. The water contact angle of HCPs studied here was 113°, and with azobenzene in HCP pores, the WCA of HCPs@Azo increased to 127°. This was ascribed to the hydrophobic nature of azobenzene [28] which enhanced hydrophobicity [47]. In addition, the WCA of HCPs@Azo that were immersed in water for 24 h was 125°. This was similar to the WCA of pristine HCPs@Azo, indicating that water molecules did not displace azobenzene molecules from HCP pores.

This was validated with XPS and elemental analyses (Table S2, Fig. 2d, Figure S3) where N content remained unchanged in pristine and water-soaked HCPs@Azo samples. The small differences in N content

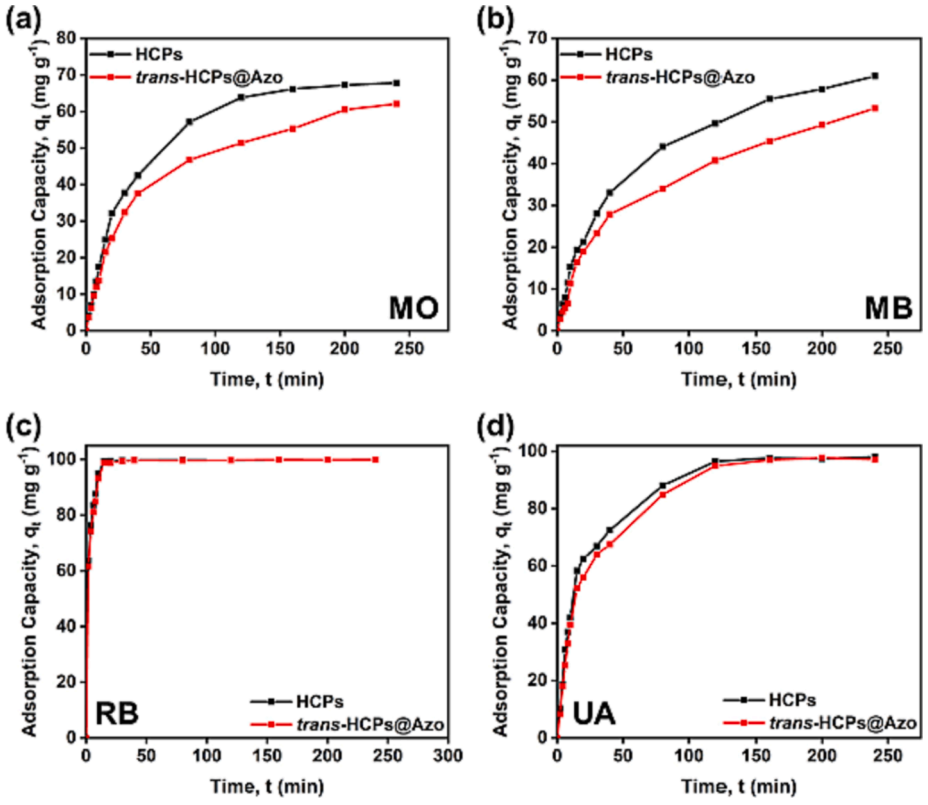


**Fig. 4.** Adsorption kinetics from 2 min to 240 min of HCPs (black) and *trans*-HCPs@Azo (red) for 10 mL dyes solutions at initial concentration of 100 mg $L^{-1}$: (a) MO, (b) MB, (c) RB and (d) UA. (For interpretation of the references to color in this figure legend, the reader is referred to the web version of this article.)

**Table 2**
The parameters of Pseudo-first-order and Pseudo-second-order models for MO, MB, RB and UA adsorbed by HCPs and *trans*-HCPs@Azo. (initial concentration: 100 mg $L^{-1}$).

| Kinetic models | Parameters | MO | MB | RB | UA |
|---|---|---|---|---|---|
| HCPs | $q_{e,\ exp}$ (mg $g^{-1}$) | 70.2 | 68.4 | 100 | 98.3 |
| Pseudo-first-order | $q_{e,\ cal}$ (mg $g^{-1}$) | 56.4 | 57.8 | 4.0 | 68.6 |
| | $k_1$ (1/min) | 0.015 | 0.0089 | 0.019 | 0.025 |
| | $R^2$ | 0.966 | 0.982 | 0.489 | 0.965 |
| Pseudo-second-order | $q_{e,\ cal}$ (mg $g^{-1}$) | 79.6 | 70 | 100.3 | 105.4 |
| | $k_2$ (g/mg·min) | $3.5 \times 10^{-4}$ | $3.4 \times 10^{-4}$ | 0.015 | $6.1 \times 10^{-4}$ |
| | $R^2$ | 0.997 | 0.996 | 0.999 | 0.999 |
| *trans*-HCPs@Azo | $q_{e,\ exp}$ (mg $g^{-1}$) | 62.5 | 58.6 | 100 | 97.7 |
| Pseudo-first-order | $q_{e,\ cal}$ (mg $g^{-1}$) | 59.5 | 51.7 | 5.7 | 73.4 |
| | $k_1$ (1/min) | 0.017 | 0.009 | 0.022 | 0.024 |
| | $R^2$ | 0.95 | 0.984 | 0.615 | 0.957 |
| Pseudo-second-order | $q_{e,\ cal}$ (mg $g^{-1}$) | 70.9 | 62.3 | 100.4 | 106.6 |
| | $k_2$ (g/mg·min) | $3.6 \times 10^{-4}$ | $3.0 \times 10^{-4}$ | 0.012 | $4.9 \times 10^{-4}$ |
| | $R^2$ | 0.997 | 0.985 | 0.999 | 0.999 |

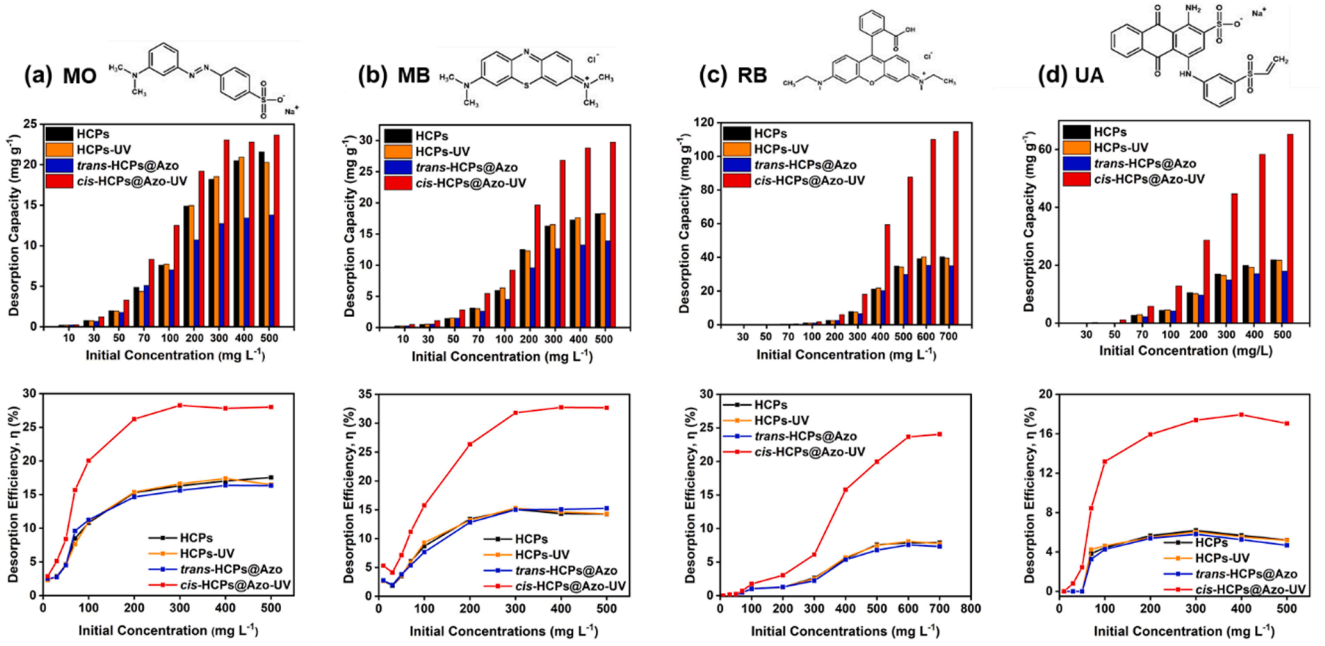


**Fig. 5.** Desorption capacities and efficiencies of HCPs (black), *trans*-HCPs@Azo (blue) without UV irradiation in water and HCPs-UV (orange), *cis*-HCPs@Azo-UV (red) with UV irradiation in water for (a) MO, (b) MB, (c) RB and (d) UA of the initial concentration from 10 mg $L^{-1}$ to 500 mg $L^{-1}$ (700 mg $L^{-1}$ for RB only). (For interpretation of the references to color in this figure legend, the reader is referred to the web version of this article.)

obtained from XPS and elemental analyses were due to the different measurement mechanism between these techniques. Elemental analysis depended on combustion to convert all elements to gaseous states [48] while XPS is a surface sensitivity analysis technique that could only determine the elemental ratio on sample surfaces [49,50].

### 4.2. Photo-modulated adsorption and kinetics

The dye (MO, MB, RB, and UA) adsorption capacities of HCPs used here were identical to those reported in our previous work [17]. Fig. 3 showed that HCP adsorption capacities for MO, MB, RB, and UA increased from 9.1 mg $g^{-1}$ to 123 mg $g^{-1}$, 9.4 mg $g^{-1}$ to 128 mg $g^{-1}$, 10 mg $g^{-1}$ to 510.4 mg $g^{-1}$ and 10 mg $g^{-1}$ to 419.5 mg $g^{-1}$, respectively, as the initial dye concentration in water increased from 10 mg $L^{-1}$ to 500 mg $L^{-1}$ (700 mg $L^{-1}$ for RB). The dye adsorption capacities of *trans*-HCPs@Azo also increased from 8.7 mg $g^{-1}$ to 84.5 mg $g^{-1}$ (MO), 9.4 mg $g^{-1}$ to 91 mg $g^{-1}$ (MB), 10 mg $g^{-1}$ to 477.1 mg $g^{-1}$ (RB) and 10 mg $g^{-1}$ to 383 mg $g^{-1}$ (UA). The increased adsorption capacities were attributed to the enhanced interactive attraction between more dyes with adsorbents [51]. As both HCPs and HCPs@Azo were synthesized from polystyrene, the π–electrons from unsaturated benzene rings could form strong π–π interactions with other π–electrons on the unsaturated aromatic rings of these four dyes [52,53]. The higher RB and UA adsorption capacities of *trans*-HCPs@Azo could be attributed to more π–π interactions associated with the higher number of unsaturated bonds in RB and the hydrogen bonding between the amine groups of UA and aromatic rings in HCPs@Azo [17,54].

Increments in dye adsorption capacities as a function of higher dye concentrations were accompanied by reductions in adsorption efficiencies. For HCPs, the adsorption efficiency decreased from 91.1% to 24.6% (MO), 94.2% to 25.6% (MB), 100% to 72.9% (RB), and 100% to 83.9% (UA). Meanwhile, the dye adsorption efficiencies of *trans*-HCPs@Azo, reduced from 87.3% to 16.9% (MO), 94.1% to 18.2% (MB), 100% to 68.2% (RB) and 100% to 76.6% (UA). The lower adsorption efficiencies were ascribed to the saturation of adsorbents, as well as mutual repulsion between dye layers and residual dyes in solution [55]. Additionally, the smaller pore sizes of *trans*-HCPs@Azo that were partially blocked by azobenzene molecules may also lead to lower adsorption capacities and efficiencies when compared to those of pristine HCPs.

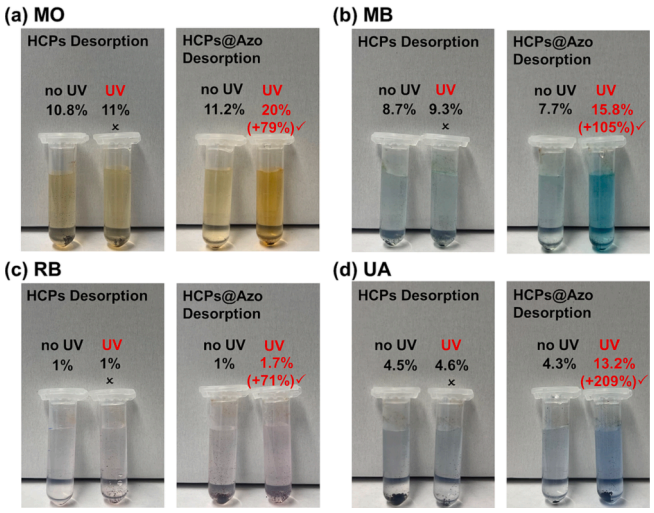


**Fig. 6.** Eluent solutions of (a) MO, (b) MB, (c) RB and (d) UA after desorption from spent HCPs (HCPs, HCPs-UV) and HCPs@Azo (*trans*-HCPs@Azo, *cis*-HCPs@Azo-UV) without/with UV irradiation into water. (initial concentration: 100 mg $L^{-1}$).

To elucidate the dye adsorption mode in HCPs and *trans*-HCPs@Azo, we fitted the experimental data with Langmuir and Freundlich isotherm models (Figure S14). The parameters obtained from both models were listed in Table 1. The higher determination coefficients ($R^2$) [56] of MO (0.997 (HCPs), 0.999 (*trans*-HCPs@Azo)), MB (0.990 (HCPs), 0.997 (*trans*-HCPs@Azo)) and RB (0.999 (HCPs), 0.999 (*trans*-HCPs@Azo)) using Langmuir model showed that this model was more appropriate for describing the adsorption processes of these dyes in HCPs and *trans*-HCPs@Azo i.e., monolayer adsorption on homogeneous surfaces. However, the higher $R^2$ value (0.998 (HCPs), 0.968 (*trans*-HCPs@Azo)) of UA was obtained using the Freudlich model, indicating that UA adsorption occurred on heterogeneous surfaces. 1/n obtained from the Freundlich isotherm is a measure for the intensity of adsorption, and the adsorption of these dyes had a value of $1/n < 1$, indicative of favorable adsorption [57]. Regardless of dye type, the description of adsorption modes in both HCPs and *trans*-HCPs@Azo could be described using the same isotherm model. This indicated that the presence of azobenzene molecules in the pores of *trans*-HCPs@Azo did not affect the adsorption mode.

The adsorption kinetics of HCPs and *trans*-HCPs@Azo were evaluated by analyzing the pseudo-first and pseudo-second-order kinetic models fitted with (Figure S15) dye adsorption data obtained from an initial concentration of 100 mg $L^{-1}$ over 2 to 240 min (Fig. 4). In comparison to the parameter calculated by the pseudo-first-order model (Table 2), the $R^2$ values obtained from the pseudo-second-order model for the adsorption of all four dyes studied here were higher. Simultaneously, the equilibrium adsorption capacities calculated from the pseudo-second-order were in better agreement with the experimental results than those from the pseudo-first-order. For these reasons, the adsorption mechanism was better described with the pseudo-second-order which depended on the adsorbent and dyes [58,59]. The comparatively smaller rate constant of pseudo-second-order ($k_2$) of *trans*-HCPs@Azo was ascribed to the presence of azobenzene molecules on/ near adsorption sites on pore walls.

### 4.3. Photo-modulated desorption and kinetics

The desorption capacities and efficiencies of materials studied here in this work were determined by quantifying the amount of dyes released from dye-loaded HCPs and HCP@Azo that were used to adsorb dyes from mixtures with different initial concentrations (Fig. 5). Desorption experiments were performed in an eluent comprising deionized water (initial concentration: 100 mg $L^{-1}$) (Fig. 6).

In control experiments, we observed a slight color change in the eluent when dye-loaded HCPs and *trans*-HCPs@Azo were immersed into water (Fig. 6). Note that these samples were not irradiated with UV light. The slight color change indicated that 10.8 %, 8.7 %, 1 % and 4.5 % of MO, MB, RB and UA dyes were desorbed from HCPs, compared to 11.2 %, 7.7 %, 1 % and 3 %, from *trans*-HCPs@Azo, respectively. For MO and MB desorption, we observed that the eluent turned orange and blue, respectively, prior UV irradiation. This could be ascribed to dissolution of dyes on the surfaces of adsorbents into water. Meanwhile for RB and UA, it was clear that HCPs and HCPs@Azo adsorbed almost all of these dyes that were present in water (Figure S16), yielding clear water. As a result, when adsorbents that were loaded with RB and UA were immersed in a water eluent, there was no obvious color change in the eluent. This showed the limited role of water during dye desorption in HCPs@Azo when UV irradiation was not present.

In a separate set of experiments, we immersed HCPs and *cis*-HCPs@Azo-UV that were loaded with dyes into deionized water, and continuously irradiated these samples with UV light for 4 h. Fig. 6 clearly showed that UV irradiation enhanced dye desorption from HCP pores. With UV stimuli, the desorption capacities, and efficiencies of *cis*-HCPs@Azo-UV were larger than those of *trans*-HCPs@Azo. Compared to *trans*-HCPs@Azo, the *cis*-HCPs@Azo-UV dye desorption efficiencies of MO, MB, RB and UA increased by 79 %, 105 %, 71 % and 209 %, respectively. Meanwhile, the desorption capacities and efficiencies of HCPs and HCPs-UV were similar. This indicated that pristine HCPs were not responsive to UV light and photo-modulated desorption only occurred in photo-responsive HCPs@Azo.

A possible reason for the increased desorption capacity of *cis*-HCPs@Azo-UV was UV-irradiation triggered an increase in accessible HCP volume due to azobenzene dimensions reducing from 9 Å to 5.5 Å during *trans*-to-*cis* photo-isomerization. The more accessible pores allowed water molecules located around the hydrophobic *cis*-HCPs@Azo-UV to come into contact with adsorbed dyes on the pore surface [60,61]. As these dyes were more soluble in water, it was highly likely that the dyes re-dissolved in water [62-65]. As azobenzene molecules are hydrophobic [28], they were more likely to retain in on the hydrophobic HCP pores.

It is important to highlight that the photo-modulated desorption efficiencies did not reach 100% i.e. dyes remain adsorbed in *cis*-HCPs@Azo-UV, even after photo-irradiation. This could be attributed to the fact that not all HCP pores contained azobenzene which was key for enabling photo-modulated desorption, where dyes could remain adsorbed within HCP pores that do not contain azobenzene. The UV-modulated desorption efficiencies of MB and MO for *cis*-HCPs@Azo-UV were higher than those of RB and UA. Here we observed that only

**Table 3**
The parameters of Langmuir and Freundlich isotherm models for MO, MB, RB and UA desorbed from HCPs, HCPs-UV, *trans*-HCPs@Azo and *cis*-HCPs@Azo-UV in 10 mL water.

| Isotherm models | Parameters | MO | MB | RB | UA |
|---|---|---|---|---|---|
| Langmuir (HCPs) | $q_{Dmax}$ (mg $g^{-1}$) | 12.6 | 13.2 | 47.2 | 20.4 |
| | $K_L$ (L/mg) | 2.28 | 2.57 | 5.52 | 3.39 |
| | $R^2$ | 0.969 | 0.954 | 0.985 | 0.631 |
| Freudlich (HCPs) | $K_F$ [(mg/g)(L/mg)$^{1/n}$] | 24.1 | 26.7 | 125.8 | 28.9 |
| | n | 2.08 | 2.09 | 2.78 | 1.24 |
| | $R^2$ | 0.966 | 0.925 | 0.975 | 0.98 |
| Langmuir (HCPs-UV) | $q_{Dmax}$ (mg $g^{-1}$) | 13.4 | 13.1 | 49.4 | 11.2 |
| | $K_L$ (L/mg) | 2.2 | 2.53 | 5.36 | 5.85 |
| | $R^2$ | 0.966 | 0.953 | 0.983 | 0.589 |
| Freudlich (HCPs-UV) | $K_F$ [(mg/g)(L/mg)$^{1/n}$] | 24.4 | 26.3 | 127.1 | 25.4 |
| | n | 2.09 | 2.08 | 2.81 | 1.16 |
| | $R^2$ | 0.963 | 0.93 | 0.978 | 0.987 |
| Langmuir (*trans*-HCPs@Azo) | $q_{Dmax}$ (mg $g^{-1}$) | 7.9 | 8.6 | 39.5 | 31.4 |
| | $K_L$ (L/mg) | 4.58 | 4.94 | 7.74 | 2.58 |
| | $R^2$ | 0.985 | 0.99 | 0.9988 | 0.657 |
| Freudlich (*trans*-HCPs@Azo) | $K_F$ [(mg/g)(L/mg)$^{1/n}$] | 22.6 | 25.7 | 128 | 32.5 |
| | | 2.21 | 2.27 | 2.81 | 1.28 |
| | n | | | | |
| | $R^2$ | 0.939 | 0.886 | 0.975 | 0.965 |
| Langmuir (*cis*-HCPs@Azo-UV) | $q_{Dmax}$ (mg $g^{-1}$) | 21.7 | 28.6 | 115.2 | 55.9 |
| | $K_L$ (L/mg) | 1.12 | 0.89 | 1.26 | 0.38 |
| | $R^2$ | 0.991 | 0.997 | 0.975 | 0.749 |
| Freudlich (*cis*-HCPs@Azo-UV) | $K_F$ [(mg/g)(L/mg)$^{1/n}$] | 18.1 | 18.8 | 93.7 | 42.2 |
| | | 2.52 | 2.65 | 3.25 | 2.43 |
| | n | | | | |
| | $R^2$ | 0.955 | 0.823 | 0.971 | 0.909 |

1.7 % and 13.2 % of RB and UA that were adsorbed in *cis*-HCPs@Azo-UV were desorbed upon UV irradiation, while 15.8 % and 20 % of MB and MO were desorbed. This could be ascribed to the stronger π–π interactions and hydrogen bonds between HCPs and RB and UA [17].

Photo-modulated dye desorption of HCPs, *trans*-HCPs@Azo, HCPs-UV, and *cis*-HCPs@Azo-UV in water was evaluated using the Langmuir and Freundlich isotherm models (Figure S17, Table 3). With higher $R^2$ values when compared to those obtained from the Freundlich model, the desorption of MO, MB, and RB in these adsorbents was better described using the Langmuir model i.e., desorption occurred on homogeneous surfaces without interactions between adsorbed dyes and neighbouring active sites. The experimental data for UA desorption fitted better with the Freundlich model, indicating that UA desorption was non-ideal, with interactions between adsorbed molecules [2]. It was worth noting that UV irradiation did not affect desorption isotherm models, inferring that UV irradiation only improved desorption capacities but did not generate new reactions to alter desorption mode.

Desorption kinetics is crucial for adsorbent regeneration [66]. Here we fitted the experimental dye desorption data of HCPs and HCP@Azo with/without UV irradiation with the pseudo-first and pseudo-second-order kinetic models (Fig. 7, Figure S18). Regardless of dye types and higher determinate $R^2$, the pseudo-second-order model was a better fit for explaining desorption kinetics in these adsorbents (Table 4). Meanwhile, experimental, and theoretical $q_e$ values were identical, fitting well with the pseudo-second-order model. Clearly, dye desorption in HCPs and HCP@Azo was the rate-limiting step and depended on adsorbents [67]. Moreover, regardless of dye types, the rate constant of the pseudo-second-order ($k_2$) for *cis*-HCPs@Azo-UV was larger than that of *trans*-HCPs@Azo i.e., faster desorption rates [68]. This could be ascribed to larger accessible pore volumes in *cis*-HCPs@Azo-UV upon UV irradiation. The desorption rate of UV-triggered *cis*-HCPs@Azo-UV was higher than that of pristine HCPs. This was also because with more accessible pore volume (UV-induced) in *cis*-HCPs@Azo-UV, contact between water molecules and adsorbed dyes could be enhanced, leading to faster desorption rates. Meanwhile the accessible pore volume of pristine HCPs remained unchanged upon UV-irradiation. This limited interactions

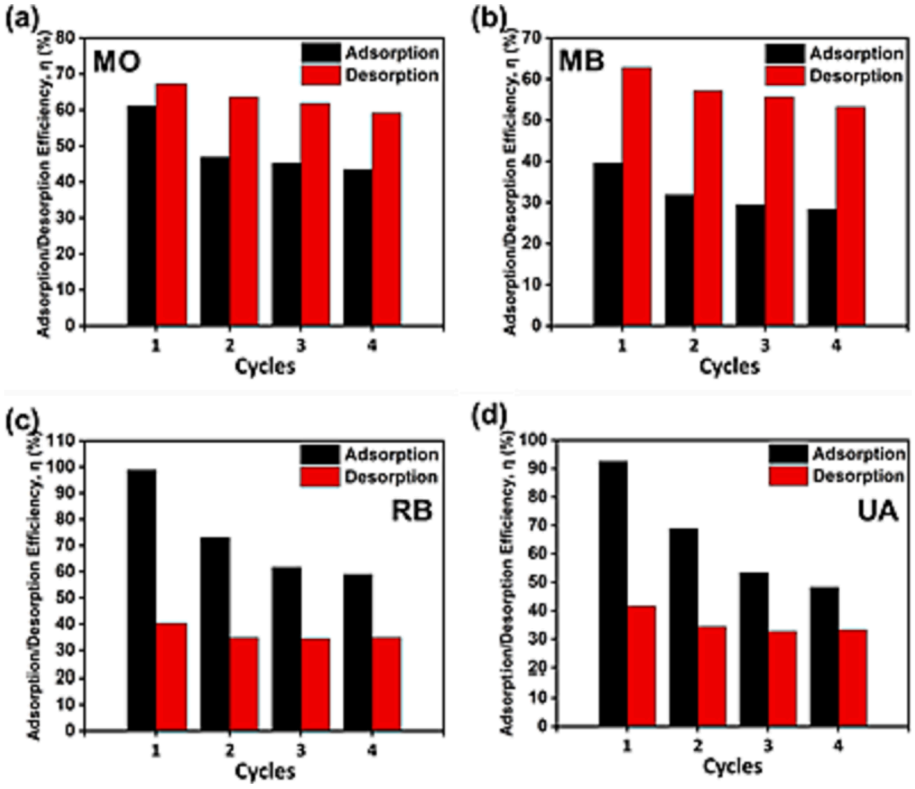


**Fig. 7.** Desorption kinetics for four dyes from 2 min to 160 min of spent HCPs (black) /*trans*-HCPs@Azo (blue) without UV irradiation in 10 mL water and HCPs-UV (orange) /*cis*-HCPs@Azo-UV (red) with UV irradiation in 10 mL water (dyes concentration: 100 mg $L^{-1}$, dyes volume: 10 mL, mass of adsorbents: 10 mg): (a) MO, (b) MB, (c) RB and (d) UA. (For interpretation of the references to color in this figure legend, the reader is referred to the web version of this article.)

**Table 4**
The parameters of Pseudo-first-order and Pseudo-second-order models for MO, MB, RB and UA desorbed from HCPs, HCPs-UV, *trans*-HCPs@Azo and *cis*-HCPs@Azo-UV in 10 mL water (initial concentration for adsorption: 100 mg $L^{-1}$).

| Kinetic models | Parameters | MO | MB | RB | UA |
|---|---|---|---|---|---|
| HCPs | $q_{e,\ exp}$ (mg $g^{-1}$) | 7.6 | 5.94 | 1.05 | 4.38 |
| Pseudo-first-order | $q_{e,\ cal}$ (mg $g^{-1}$) | 3.76 | 2.5 | 0.3 | 0.338 |
| | $k_1$ (1/min) | 0.034 | 0.0195 | 0.02 | 0.02 |
| | $R^2$ | 0.898 | 0.844 | 0.660 | 0.283 |
| Pseudo-second-order | $q_{e,\ cal}$ (mg $g^{-1}$) | 8.1 | 5.98 | 1.05 | 4.43 |
| | $k_2$ (g/mg·min) | 0.014 | 0.029 | 0.284 | 0.315 |
| | $R^2$ | 0.997 | 0.999 | 0.999 | 0.999 |
| HCPs-UV | $q_{e,\ exp}$ (mg $g^{-1}$) | 7.74 | 6.36 | 1.05 | 4.55 |
| Pseudo-first-order | $q_{e,\ cal}$ (mg $g^{-1}$) | 4.39 | 3.1 | 0.27 | 0.492 |
| | $k_1$ (1/min) | 0.034 | 0.016 | 0.025 | 0.008 |
| | $R^2$ | 0.921 | 0.885 | 0.51 | 0.268 |
| Pseudo-second-order | $q_{e,\ cal}$ (mg $g^{-1}$) | 8.27 | 6.3 | 1.06 | 4.38 |
| | $k_2$ (g/mg·min) | 0.012 | 0.021 | 0.263 | 0.356 |
| | $R^2$ | 0.999 | 0.999 | 0.999 | 0.999 |
| *trans*-HCPs@Azo | $q_{e,\ exp}$ (mg $g^{-1}$) | 7.03 | 4.49 | 1.02 | 4.18 |
| Pseudo-first-order | $q_{e,\ cal}$ (mg $g^{-1}$) | 3.93 | 2.24 | 0.265 | 0.238 |
| | $k_1$ (1/min) | 0.03 | 0.026 | 0.022 | 0.022 |
| | $R^2$ | 0.942 | 0.97 | 0.521 | 0.514 |
| Pseudo-second-order | $q_{e,\ cal}$ (mg $g^{-1}$) | 7.49 | 4.62 | 1.05 | 4.19 |
| | $k_2$ (g/mg·min) | 0.013 | 0.032 | 0.257 | 0.45 |
| | $R^2$ | 0.999 | 0.999 | 0.999 | 0.999 |
| *cis*-HCPs@Azo-UV | $q_{e,\ exp}$ (mg $g^{-1}$) | 12.52 | 9.23 | 1.74 | 12.87 |
| Pseudo-first-order | $q_{e,\ cal}$ (mg $g^{-1}$) | 3.03 | 2.28 | 0.232 | 0.708 |
| | $k_1$ (1/min) | 0.019 | 0.021 | 0.012 | 0.005 |
| | $R^2$ | 0.56 | 0.755 | 0.108 | 0.067 |
| Pseudo-second-order | $q_{e,\ cal}$ (mg $g^{-1}$) | 12.7 | 9.27 | 1.7 | 12.57 |
| | $k_2$ (g/mg·min) | 0.019 | 0.036 | 0.312 | 0.53 |
| | $R^2$ | 0.999 | 0.999 | 0.999 | 0.999 |

between water molecules and dye molecules present in HCP pores.

### 4.4. Reusability

We exploited UV irradiation to desorb dyes from adsorbents, yielding *cis*-HCPs@Azo-UV, and used visible light to revert these adsorbents to *trans*-HCPs@Azo for reuse. The adsorption and desorption efficiencies, and accumulated dyes in HCPs@Azo of four repeated adsorption/desorption cycles are shown in Fig. 8 and Figure S19. From the first to third cycle, the adsorption efficiencies for all dyes were reduced (MO: 61 % to 45 %, MB: 40 % to 28 %, RB: 99 % to 62 %, UA: 93 % to 53 %). In the fourth cycle, the reductions in adsorption efficiencies were relatively smaller when compared to the first three times (MO: 43 %, MB: 28 %, RB: 59 %, UA: 48 %). This was because some dyes remained adsorbed on the binding sites of HCPs@Azo, reducing adsorption efficiency [35]. The desorption efficiencies of four dyes were only slightly reduced after four cycles (MO: 67 % to 59 %, MB: 63 % to 53 %, RB: 40 % to 35 %, UA: 41 % to 33 %. This indicated an equilibrium-oriented adsorption–desorption process and good regeneration properties and reusability of HCPs@Azo.

From FTIR analyses, we observed that there were no changes in characteristic peak positions of HCPs@Azo after cyclic testing [Figure S5-S9], indicating that chemical stability of these adsorbents even after cyclic testing. We also observed peaks that were unique to azobenzene, at 690 $cm^{-1}$ (the vibrations of monosubstituted benzenes) and 775 $cm^{-1}$ (the out-of-plane bending of C–H in benzene rings on azobenzene) [69,70] were present after adsorption and UV irradiated dye desorption. These results indicated the good stability and reusability of HCPs@Azo in dye removal, which was also validated by similar textural morphology as shown in SEM micrographs (Figures S10–S12).

From the FTIR spectra of HCPs@Azo after adsorbing dyes (Figure S6-S9), we observed the presence of peaks characteristic to the dyes used here −880 $cm^{-1}$, aromatic skeletal of four dyes [71]; 1030–1045 $cm^{-1}$

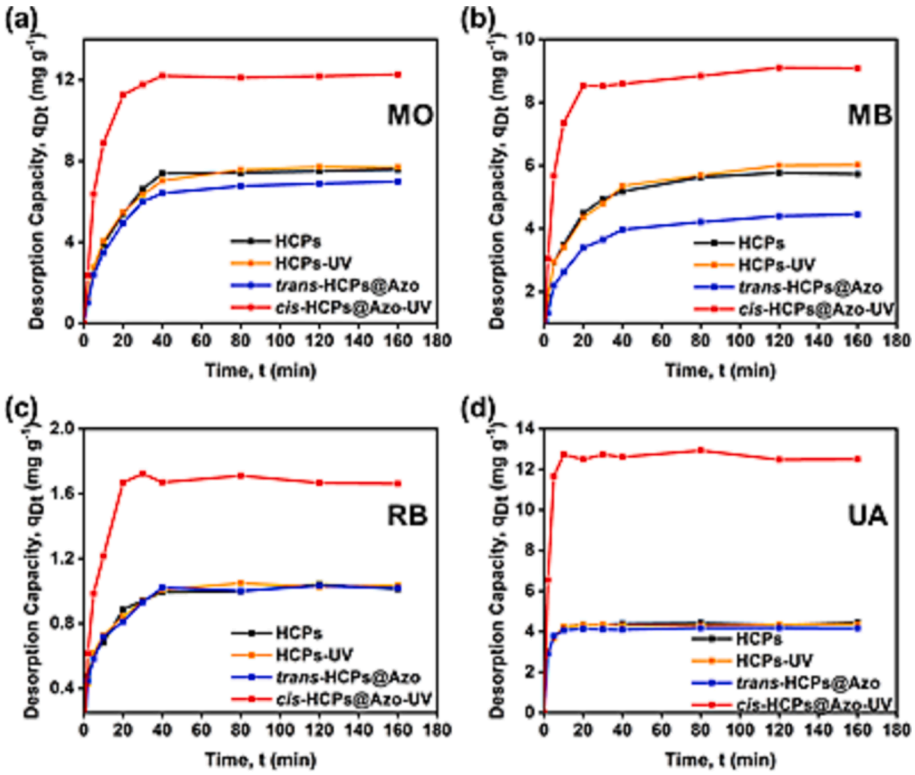


**Fig. 8.** Adsorption (black) /desorption (red) efficiency of four cycles of (a) MO, (b) MB, (c) RB and (d) UA onto/from HCPs@Azo (adsorption by *trans*-HCPs@Azo, desorption from *cis*-HCPs@Azo-UV, dyes concentration: 10 mg $L^{-1}$, dyes volume: 10 mL, water volume: 10 mL, mass of adsorbents: 10 mg). (For interpretation of the references to color in this figure legend, the reader is referred to the web version of this article.)

**Table 5**
Comparison of adosprtion and desorption performances of different adsorbent and adsorbate (dye) types.

| | Adsorbent | Adsorbent type | Adsorption capacity (mg $g^{-1}$) | Desorption method | Desorption efficiency | Ref |
|---|---|---|---|---|---|---|
| Dye type – Methyl Orange (MO) | HCPs@Azo | HCPs | 86.5 | Photo-modulation in water | 20% | This work |
| | HCPs | HCPs | 127 | Solvent (Methanol) | 41% | This work |
| | CCM | Carbonaceous materials | 102 | Solvent (NaOH) | 67% | [80] |
| Dye type – Methyl Orange (MO) | Silkworm exuviae | Biomass | 87 | Solvent (NaOH) | 17% | [81] |
| | Date pits activated carbon | Activated carbon | 434 | Water | 10% | [82] |
| | $C_{KIT-6}$ | MOFs | 260 | Solvent (NaOH) | 70% | [83] |
| | ZnBDC/CSC | MOFs | 202 | Solvent (NaOH) | 84% | [84] |
| Dye type – Methylene Blue (MB) | HCPs@Azo | HCPs | 93 | Photo-modulation in water | 16% | This work |
| | HCPs | HCPs | 131 | Solvent (methanol) | 30% | This work |
| | m-BOC | $Bi_2O_2CO_3$ nanosheets | 35 | Photo-modulation in water | 79% | [25] |
| | Marine macroalga | Biomass | 95 | Water | 2.4% | [39] |
| | CM | Monolithic carbon | 127 | Solvent (ethanol) | 50% | [85] |
| | AM-3 | Silica | 31 | Photo-modulation + Solvent (ethanol) | 100% | [23] |
| | ZSM-5 | Zeolite | 270 | Solvent (HCl) | 35% | [86] |
| | CP13 | Activated carbon | 770 | Solvent (HCl) | 42% | [87] |
| | FCBAC | Activated carbon | 48 | Solvent (HCl) | 84% | [88] |
| | SAC | Activated carbon | 263 | Heating (300 °C) | 95% | [20] |
| | HKUST-1/GO | MOFs/GO | 183 | Solvent (acetone) | 90% | [89] |
| | HCPS-OH-4 | HCPs | 294 | Solvent (HCl, methanol) | 92% | [90] |
| Dye type – Rhodamine B (RB) | HCPs@Azo | HCPs | 377 | Photo-modulation in water | 1.7% | This work |
| | HCPs | HCPs | 407 | Solvent (methanol) | 23% | This work |
| | MCM-41 NPs | Mesoporous silica | – | Photo-modulation in water | 90% | [24] |
| | BPH | Activated carbon | 264 | Solvent (NaOH) | 7.8% | [91] |
| | PLA/AC 5% wt. beads | Activated carbon | 150 | Solvent (HCl) | 47% | [92] |
| | TPC | Activated carbon | 61 | Solvent (HCl) | 79% | [93] |
| | GO/PNA-2 | Hydrogel | 193 | Solvent (HCl) | 81% | [94] |
| | HP8 | HCPs | 420 | Solvent (ethanol) | 99% | [95] |
| Dye type – UniBlue A (UA) | HCPs@Azo | HCPs | 377 | Photo-modulation in water | 13% | This work |
| | HCPs | HCPs | 407 | Solvent (methanol) | 38% | This work |

and 1600 $cm^{-1}$, S = O stretching vibrations in MO and UA [72-74]; 1590 $cm^{-1}$, C = C and C = N stretching vibrations in MB [75]; 1085 $cm^{-1}$ and 1045 $cm^{-1}$, C-O of RB [76]. This confirmed the presence of dyes in HCPs@Azo, even after UV-irradiated desorption.

### 4.5. Performance comparison

The UV-modulated desorption performances of MO, MB, RB, and UA from photo-sensitive HCPs@Azo were comparable to those obtained from methanol regeneration of as-prepared HCPs [Figure S20]. Here it is important to reiterate that we were unable to use the approach of methanol regeneration with HCPs@Azo as the guest azobenzene molecules could be easily leached out due to azobenzene solubility in methanol [77,78]. Using methanol to desorb dyes from pristine HCPs, the desorption efficiency of the four dyes reached 22.6–40.5%. Meanwhile, the use of UV-irradiation triggered the desorption efficiency of 20 %, 15.8 %, and 13.2 % of MO, MB, and UA from HCPs@Azo. For MO and MB, this was 50 % more dyes being desorbed when compared to the traditional method of methanol desorption. This indicated the feasibility of photo-induced desorption is a feasible method and worth considering to replace traditional desorption methods in the further study, especially when considering its advantages of economy and environmental protection.

Here we compare the desorption capacities of adsorbents reported in literature for the four dye types studied in this work (Table 5). The dye desorption efficiencies of such adsorbents were higher than those of HCPs@Azo. This was because most reported works use the highly efficient solvent or thermal approaches to drive desorption. However, the limitations of solvent- and thermal-driven desorption – generation of solvent waste and high energy consumption, respectively, must be addressed for establishing a low-carbon, zero-waste water treatment technology.

An approach to concomitantly reduce both waste generation and high energy consumption of desorption is to use photo-irradiation to drive this process. For example, $Bi_2O_2CO_3$ nanosheets that utilise UV light to desorb 79 % of adsorbed Methylene Blue [25]. This desorption capacity is significantly higher than that of HCPs@Azo (16 %). However, the MB adsorption capacity of $Bi_2O_2CO_3$ nanosheets only reached

35 mg $g^{-1}$, 2.6-fold lower than that of HCPs@Azo (93 mg $g^{-1}$). Like reported adsorbents, the desorption capacities of HCPs@Azo should be further improved, and this could be achieved by ensuring that all HCP pores are decorated with azobenzene. Currently there is only a maximum of 8.9 wt% of azobenzene loaded into HCP pores. This could be delivered by grafting functionalised azobenzene on to HCP pores containing active sites for e.g., HCPs derived from aniline [79]. Nonetheless, here we show that the concept of photo-modulating dye desorption from adsorbents in water is feasible and can potentially pave the route towards a zero-carbon, zero-waste water treatment technology.

## 5. Conclusion

We proved the feasibility of using light-controlled mechanisms to induce dye desorption from HCP-based adsorbents for water treatment. Visible light irradiated *trans*-HCPs@Azo adsorbed different dyes – MO, MB, RB, and UA of different concentrations in water. At 100 mg $L^{-1}$, the adsorption efficiency for MO, MB, RB, and UA was 62.5 %, 58.6 %, 100 %, and 97.7%, respectively. UV-irradiation of dye-loaded HCP@Azo desorbed 20 %, 15.8 %, 1.7 % and 13.2 % of MO, MB, RB, and UA adsorbed, respectively. The dye desorption rates could be potentially enhanced by increasing the azobenzene content in the adsorbent. The adsorption/desorption isotherms of MO, MB, and RB fitted better with the Langmuir model while those of UA were more suitable to the Freundlich model. Adsorption and desorption kinetics of all four dyes studied here could be described by the Pseudo-second-order model, and a higher rate constant $k_2$ indicated UV light could improve the desorption rate. Four stable and consecutive adsorption–desorption cycles proved HCPs@Azo adsorbents had good reusability. In summary, we validated the feasibility of photo-modulated regeneration of adsorbents, but desorption efficiency should be improved before potential applications in the industry.

## CRediT authorship contribution statement

**Aotian Liu:** Conceptualization, Methodology, Software, Validation, Formal analysis, Investigation, Data curation, Writing – original draft, Writing – review & editing, Visualization. **Xiuming Wei:** Investigation, Formal analysis, Data curation, Software. **Shiliang Lin:** Validation, Investigation. **Liang Ding:** Software, Validation. **Yi Huang:** Resources, Writing – review & editing. **Xianfeng Fan:** Resources, Writing – review & editing. **Pei Li:** Resources, Writing – review & editing, Supervision. **Cher Hon Lau:** Resources, Writing – review & editing, Supervision, Project administration.

## Declaration of Competing Interest

The authors declare that they have no known competing financial interests or personal relationships that could have appeared to influence the work reported in this paper.

## Data availability

Data will be made available on request.

## Acknowledgments

The authors would like to thank the School of Materials Science and Engineering, Beijing University of Chemical Technology for the support and assistance in characterization. We also acknowledge Mr. Joe Casillo for elemental analysis.

## Appendix A. Supplementary data

Supplementary data to this article can be found online at https://doi.org/10.1016/j.seppur.2023.125142.

## References

[1] K.B. Tan, M. Vakili, B.A. Horri, P.E. Poh, A.Z. Abdullah, B. Salamatinia, Adsorption of dyes by nanomaterials: recent developments and adsorption mechanisms, Sep. Purif. Technol. 150 (2015) 229–242.
[2] S. Mohammad, I. Suzylawati, Study of the adsorption/desorption of MB dye solution using bentonite adsorbent coating, J. Water Process Eng. 34 (2020), 101155.
[3] V. Gomez, M. Larrechi, M. Callao, Kinetic and adsorption study of acid dye removal using activated carbon, Chemosphere 69 (2007) 1151–1158.
[4] G. Zhang, L. Yi, H. Deng, P. Sun, Dyes adsorption using a synthetic carboxymethyl cellulose-acrylic acid adsorbent, J. Environ. Sci. 26 (2014) 1203–1211.
[5] R. Kecili, C.M. Hussain, Mechanism of adsorption on nanomaterials, in: Nanomaterials in chromatography, Elsevier, 2018, pp. 89–115.
[6] D. Wang, Y. Li, D. Li, Y. Xia, J. Zhang, A review on adsorption refrigeration technology and adsorption deterioration in physical adsorption systems, Renew. Sustain. Energy Rev. 14 (2010) 344–353.
[7] H. Margenau, Van der Waals forces, Rev. Mod. Phys. 11 (1939) 1.
[8] Y. El Maguana, N. Elhadiri, M. Benchanaa, R. Chikri, Activated carbon for dyes removal: modeling and understanding the adsorption process, J. Chem. 2020 (2020) 1–9.
[9] Q. Shi, J. Zhang, C. Zhang, C. Li, B. Zhang, W. Hu, J. Xu, R. Zhao, Preparation of activated carbon from cattail and its application for dyes removal, J. Environ. Sci. 22 (2010) 91–97.
[10] N. Yang, S. Zhu, D. Zhang, S. Xu, Synthesis and properties of magnetic Fe3O4-activated carbon nanocomposite particles for dye removal, Mater. Lett. 62 (2008) 645–647.
[11] S. Wang, Z. Zhu, Characterisation and environmental application of an Australian natural zeolite for basic dye removal from aqueous solution, J. Hazard. Mater. 136 (2006) 946–952.
[12] S. Wang, H. Li, L. Xu, Application of zeolite MCM-22 for basic dye removal from wastewater, J. Colloid Interface Sci. 295 (2006) 71–78.
[13] E. Haque, J.W. Jun, S.H. Jhung, Adsorptive removal of methyl orange and methylene blue from aqueous solution with a metal-organic framework material, iron terephthalate (MOF-235), J. Hazard. Mater. 185 (2011) 507–511.
[14] C. Arora, S. Soni, S. Sahu, J. Mittal, P. Kumar, P. Bajpai, Iron based metal organic framework for efficient removal of methylene blue dye from industrial waste, J. Mol. Liq. 284 (2019) 343–352.
[15] F. Liu, S. Chung, G. Oh, T.S. Seo, Three-dimensional graphene oxide nanostructure for fast and efficient water-soluble dye removal, ACS Appl. Mater. Interfaces 4 (2012) 922–927.
[16] B. Mao, B. Sidhureddy, A.R. Thiruppathi, P.C. Wood, A. Chen, Efficient dye removal and separation based on graphene oxide nanomaterials, New J. Chem. 44 (2020) 4519–4528.
[17] X. Dong, A. Akram, B. Comesaña-Gándara, X. Dong, Q. Ge, K. Wang, S.-P. Sun, B. Jin, C.H. Lau, Recycling plastic waste for environmental remediation in water purification and CO2 capture, ACS Appl. Polym. Mater. 2 (2020) 2586–2593.
[18] D.S.d.C. Coltre, C.A. Cionek, J.G. Meneguin, C.H. Maeda, M.U.C. Braga, A.C. de Araújo, G.d.F. Gauze, M.A.S.D. de Barros, P.A. Arroyo, Study of dye desorption mechanism of bone char utilizing different regenerating agents, SN Appl. Sci., 2 (2020) 1-14.
[19] H. Patel, Review on solvent desorption study from exhausted adsorbent, J. Saudi Chem. Soc. 25 (2021), 101302.
[20] W.-H. Li, Q.-Y. Yue, B.-Y. Gao, Z.-H. Ma, Y.-J. Li, H.-X. Zhao, Preparation and utilization of sludge-based activated carbon for the adsorption of dyes from aqueous solutions, Chem. Eng. J. 171 (2011) 320–327.
[21] A.A. Alqadami, M. Naushad, Z. Alothman, T. Ahamad, Adsorptive performance of MOF nanocomposite for methylene blue and malachite green dyes: kinetics, isotherm and mechanism, J. Environ. Manage. 223 (2018) 29–36.
[22] B. Liu, M. Liu, Z. Xie, Y. Li, A. Zhang, Performance of defective Zr-MOFs for the adsorption of anionic dyes, J. Mater. Sci. 57 (2022) 5438–5455.
[23] L. Cheng, Y. Jiang, N. Yan, S.-F. Shan, X.-Q. Liu, L.-B. Sun, Smart adsorbents with photoregulated molecular gates for both selective adsorption and efficient regeneration, ACS Appl. Mater. Interfaces 8 (2016) 23404–23411.
[24] D.P. Ferris, Y.-L. Zhao, N.M. Khashab, H.A. Khatib, J.F. Stoddart, J.I. Zink, Light-operated mechanized nanoparticles, J. Am. Chem. Soc. 131 (2009) 1686–1688.
[25] H. Liu, M. Chen, D. Wei, Y. Ma, F. Wang, Q. Zhang, J. Shi, H. Zhang, J. Peng, G. Liu, Smart removal of dye pollutants via dark adsorption and light desorption at recyclable Bi2O2CO3 nanosheets interface, ACS Appl. Mater. Interfaces 12 (2020) 20490–20499.
[26] R. Ou, H. Zhang, V.X. Truong, L. Zhang, H.M. Hegab, L. Han, J. Hou, X. Zhang, A. Deletic, L. Jiang, A sunlight-responsive metal–organic framework system for sustainable water desalination, Nat. Sustainability 3 (2020) 1052–1058.
[27] A. Liu, C. Mollart, A. Trewin, X. Fan, C.H. Lau, Photo-modulating CO2 uptake of hypercross-linked polymers upcycled from polystyrene waste, ChemSusChem, (2023) e202300019.
[28] N. Ma, Y. Wang, Z. Wang, X. Zhang, Polymer micelles as building blocks for the incorporation of azobenzene: Enhancing the photochromic properties in layer-by-layer films, Langmuir 22 (2006) 3906–3909.
[29] H.D. Bandara, S.C. Burdette, Photoisomerization in different classes of azobenzene, Chem. Soc. Rev. 41 (2012) 1809–1825.
[30] K. Tsuda, G.C. Dol, T. Gensch, J. Hofkens, L. Latterini, J. Weener, E. Meijer, D. Schryver, Fluorescence from azobenzene functionalized poly (propylene imine)

dendrimers in self-assembled supramolecular structures, J. Am. Chem. Soc. 122 (2000) 3445–3452.
[31] K. Müller, J. Wadhwa, J.S. Malhi, L. Schöttner, A. Welle, H. Schwartz, D. Hermann, U. Ruschewitz, L. Heinke, Photoswitchable nanoporous films by loading azobenzene in metal–organic frameworks of type HKUST-1, Chem. Commun. 53 (2017) 8070–8073.
[32] D.F. Swinehart, The beer-lambert law, J. Chem. Educ. 39 (1962) 333.
[33] D. Yaseen, M. Scholz, Textile dye wastewater characteristics and constituents of synthetic effluents: a critical review, Int. J. Environ. Sci. Technol. 16 (2019) 1193–1226.
[34] Z. Wang, K. Müller, M. Valášek, S. Grosjean, S. Bräse, C. Wöll, M. Mayor, L. Heinke, Series of photoswitchable azobenzene-containing metal–organic frameworks with variable adsorption switching effect, J. Phys. Chem. C 122 (2018) 19044–19050.
[35] H. Chong, C. Nie, L. Wang, S. Wang, Y. Han, Y. Wang, C. Wang, C. Yan, Construction and investigation of photo-switch property of azobenzene-bridged pillar [5] arene-based [3] rotaxanes, Chin. Chem. Lett. 32 (2021) 57–61.
[36] I. Langmuir, The constitution and fundamental properties of solids and liquids II. Liquids, J. Am. Chem. Soc. 39 (1917) 1848–1906.
[37] H. Freundlich, Über die adsorption in lösungen, Z. Phys. Chem. 57 (1907) 385–470.
[38] J. Huang, X. Jin, J. Mao, B. Yuan, R. Deng, S. Deng, Synthesis, characterization and adsorption properties of diethylenetriamine-modified hypercrosslinked resins for efficient removal of salicylic acid from aqueous solution, J. Hazard. Mater. 217 (2012) 406–415.
[39] E. Daneshvar, A. Vazirzadeh, A. Niazi, M. Kousha, M. Naushad, A. Bhatnagar, Desorption of methylene blue dye from brown macroalga: effects of operating parameters, isotherm study and kinetic modeling, J. Clean. Prod. 152 (2017) 443–453.
[40] S.K. Lagergren, About the theory of so-called adsorption of soluble substances, Sven, Vetenskapsakad. Handingarl 24 (1898) 1–39.
[41] J.-P. Simonin, On the comparison of pseudo-first order and pseudo-second order rate laws in the modeling of adsorption kinetics, Chem. Eng. J. 300 (2016) 254–263.
[42] Y.S. Ho, G. McKay, A comparison of chemisorption kinetic models applied to pollutant removal on various sorbents, Process Saf. Environ. Prot. 76 (1998) 332–340.
[43] T.R. Sahoo, B. Prelot, Adsorption processes for the removal of contaminants from wastewater: the perspective role of nanomaterials and nanotechnology, in: Nanomaterials for the detection and removal of wastewater pollutants, Elsevier, 2020, pp. 161-222.
[44] J.-Y. Tseng, C.-Y. Chang, C.-F. Chang, Y.-H. Chen, C.-C. Chang, D.-R. Ji, C.-Y. Chiu, P.-C. Chiang, Kinetics and equilibrium of desorption removal of copper from magnetic polymer adsorbent, J. Hazard. Mater. 171 (2009) 370–377.
[45] Y.-S. Ho, A.E. Ofomaja, Pseudo-second-order model for lead ion sorption from aqueous solutions onto palm kernel fiber, J. Hazard. Mater. 129 (2006) 137–142.
[46] D. Ahmad, I. Van Den Boogaert, J. Miller, R. Presswell, H. Jouhara, Hydrophilic and hydrophobic materials and their applications, Energy Sources Part A 40 (2018) 2686–2725.
[47] Z. Liu, J.T. Robinson, X. Sun, H. Dai, PEGylated nanographene oxide for delivery of water-insoluble cancer drugs, J. Am. Chem. Soc. 130 (2008) 10876–10877.
[48] M.F. Gazulla, M. Rodrigo, M. Orduña, C.M. Gómez, Determination of carbon, hydrogen, nitrogen and sulfur in geological materials using elemental analysers, Geostand. Geoanal. Res. 36 (2012) 201–217.
[49] F.A. Stevie, C.L. Donley, Introduction to x-ray photoelectron spectroscopy, J. Vac. Sci. Technol. A 38 (2020).
[50] R.R. Mather, Surface modification of textiles by plasma treatments, in: Surface modification of textiles, Elsevier, 2009, pp. 296-317.
[51] E. Daneshvar, M. Kousha, M.S. Sohrabi, A. Khataee, A. Converti, Biosorption of three acid dyes by the brown macroalga Stoechospermum marginatum: isotherm, kinetic and thermodynamic studies, Chem. Eng. J. 195 (2012) 297–306.
[52] H.N. Tran, Y.-F. Wang, S.-J. You, H.-P. Chao, Insights into the mechanism of cationic dye adsorption on activated charcoal: The importance of π–π interactions, Process Saf. Environ. Prot. 107 (2017) 168–180.
[53] X. Xin, B. Chen, M. Yang, S. Gao, H. Wang, W. Gu, X. Li, B. Zhang, A critical review on the interaction of polymer particles and co-existing contaminants: Adsorption mechanism, exposure factors, effects on plankton species, J. Hazard. Mater. 445 (2023), 130463.
[54] Q. Wang, L. Zhang, L. Hao, C. Wang, Q. Wu, Z. Wang, Phosphorous-enriched knitting aryl network polymer for the rapid and effective adsorption of aromatic compounds, J. Chromatogr. A 1575 (2018) 18–25.
[55] S. Agarwal, I. Tyagi, V.K. Gupta, N. Ghasemi, M. Shahivand, M. Ghasemi, Kinetics, equilibrium studies and thermodynamics of methylene blue adsorption on Ephedra strobilacea saw dust and modified using phosphoric acid and zinc chloride, J. Mol. Liq. 218 (2016) 208–218.
[56] N.J. Nagelkerke, A note on a general definition of the coefficient of determination, Biometrika 78 (1991) 691–692.
[57] J.C. Crittenden, N.J. Hutzler, D.G. Geyer, J.L. Oravitz, G. Friedman, Transport of organic compounds with saturated groundwater flow: Model development and parameter sensitivity, Water Resour. Res. 22 (1986) 271–284.
[58] M.R. Malekbala, M.A. Khan, S. Hosseini, L.C. Abdullah, T.S. Choong, Adsorption/desorption of cationic dye on surfactant modified mesoporous carbon coated monolith: Equilibrium, kinetic and thermodynamic studies, J. Ind. Eng. Chem. 21 (2015) 36.
[59] C. Srilakshmi, R. Saraf, Ag-doped hydroxyapatite as efficient adsorbent for removal of Congo red dye from aqueous solution: Synthesis, kinetic and equilibrium adsorption isotherm analysis, Microporous Mesoporous Mater. 219 (2016) 134–144.
[60] P. Schweng, F. Mayer, D. Galehdari, K. Weiland, R.T. Woodward, A Robust and Low-Cost Sulfonated Hypercrosslinked Polymer for Atmospheric Water Harvesting, Small 2304562 (2023) 1.
[61] G.E. Schukraft, R.T. Woodward, S. Kumar, M. Sachs, S. Eslava, C. Petit, Hypercrosslinked polymers as a photocatalytic platform for visible-light-driven CO2 photoreduction using H2O, ChemSusChem 14 (2021), 1720–1727. 1.
[62] A. Mittal, A. Malviya, D. Kaur, J. Mittal, L. Kurup, Studies on the adsorption kinetics and isotherms for the removal and recovery of Methyl Orange from wastewaters using waste materials, J. Hazard. Mater. 148 (2007) 229–240.
[63] X. Cai, S. Tan, A. Xie, M. Lin, Y. Liu, X. Zhang, Z. Lin, T. Wu, W. Mai, Conductive methyl blue-functionalized reduced graphene oxide with excellent stability and solubility in water, Mater. Res. Bull. 46 (2011) 2353–2358.
[64] P. Fisher, Review of using Rhodamine B as a marker for wildlife studies, Wildl. Soc. Bull. (1999) 318–329.
[65] M.A. Mata-Gómez, M.T. Yasui, A. Guerrero-Rangel, S. Valdés-Rodríguez, R. Winkler, Accelerated identification of proteins by mass spectrometry by employing covalent pre-gel staining with Uniblue A, PLoS One 7 (2012) e31438.
[66] H.N. Bhatti, Y. Safa, S.M. Yakout, O.H. Shair, M. Iqbal, A. Nazir, Efficient removal of dyes using carboxymethyl cellulose/alginate/polyvinyl alcohol/rice husk composite: adsorption/desorption, kinetics and recycling studies, Int. J. Biol. Macromol. 150 (2020) 861–870.
[67] E. Njikam, S. Schiewer, Optimization and kinetic modeling of cadmium desorption from citrus peels: A process for biosorbent regeneration, J. Hazard. Mater. 213 (2012) 242–248.
[68] B. Pan, B. Xing, Adsorption kinetics of 17α-ethinyl estradiol and bisphenol A on carbon nanomaterials. I. Several concerns regarding pseudo-first order and pseudo-second order models, J. Soil. Sediment. 10 (2010) 838–844.
[69] S. Yin, H. Xu, W. Shi, L. Bao, Y. Gao, Y. Song, B.Z. Tang, Preparation and optical properties of poly (4-ethynyl-4′-[N, N-diethylamino] azobenzene-co-phenylacetylene), Dyes Pigm. 72 (2007) 119–123.
[70] D.S. Volkov, O.B. Rogova, M.A. Proskurnin, Temperature dependences of IR spectra of humic substances of brown coal, Agronomy 11 (2021) 1822.
[71] Y. Zhou, A. Selvam, J.W. Wong, Evaluation of humic substances during co-composting of food waste, sawdust and Chinese medicinal herbal residues, Bioresour. Technol. 168 (2014) 229–234.
[72] G. Parshetti, A. Telke, D. Kalyani, S. Govindwar, Decolorization and detoxification of sulfonated azo dye methyl orange by Kocuria rosea MTCC 1532, J. Hazard. Mater. 176 (2010) 503–509.
[73] Y. Nie, W. Gao, C. Zhou, P. Yu, X. Song, Evaluation of ageing behaviors of asphalt binders using FTIR tests, Int. J. Pavement Res. Technol. 14 (2021) 615–624.
[74] X. Yang, Z. You, J. Mills-Beale, Asphalt binders blended with a high percentage of biobinders: Aging mechanism using FTIR and rheology, J. Mater. Civ. Eng. 27 (2015) 04014157.
[75] O.V. Ovchinnikov, A.V. Evtukhova, T.S. Kondratenko, M.S. Smirnov, V. Y. Khokhlov, O.V. Erina, Manifestation of intermolecular interactions in FTIR spectra of methylene blue molecules, Vib. Spectrosc 86 (2016) 181–189.
[76] P. Mondragón-Cortez, E. Herrera-López, E. Arriola-Guevara, G. Guatemala-Morales, Application of Fourier Transform Infrared Spectroscopy (FTIR) in combination with Attenuated Total Reflection (ATR) for rapid analysis of the tequila production process, Revista Mexicana de Ingeniería Química 21 (2022). Alim2806-Alim2806.
[77] M. Moniruzzaman, C.J. Sabey, G.F. Fernando, Synthesis of azobenzene-based polymers and the in-situ characterization of their photoviscosity effects, Macromolecules 37 (2004) 2572–2577.
[78] C. Winkler, J. Halpern, G. Brady, The cis-trans Isomerization of Azobenzene in Solution, Can. J. Res. 28 (1950) 140–155.
[79] C.H. Lau, X. Mulet, K. Konstas, C.M. Doherty, M.A. Sani, F. Separovic, M.R. Hill, C. D. Wood, Hypercrosslinked Additives for Ageless Gas-Separation Membranes, Angew. Chem. Int. Ed. 55 (2016) 1998–2001.
[80] S. Hosseini, M.A. Khan, M.R. Malekbala, W. Cheah, T.S. Choong, Carbon coated monolith, a mesoporous material for the removal of methyl orange from aqueous phase: Adsorption and desorption studies, Chem. Eng. J. 171 (2011) 1124–1131.
[81] H. Chen, J. Zhao, J. Wu, G. Dai, Isotherm, thermodynamic, kinetics and adsorption mechanism studies of methyl orange by surfactant modified silkworm exuviae, J. Hazard. Mater. 192 (2011) 246–254.
[82] K. Mahmoudi, K. Hosni, N. Hamdi, E. Srasra, Kinetics and equilibrium studies on removal of methylene blue and methyl orange by adsorption onto activated carbon prepared from date pits-A comparative study, Korean J. Chem. Eng. 32 (2015) 274–283.
[83] J. Goscianska, M. Marciniak, R. Pietrzak, Mesoporous carbons modified with lanthanum (III) chloride for methyl orange adsorption, Chem. Eng. J. 247 (2014) 258–264.
[84] C. Niu, N. Zhang, C. Hu, C. Zhang, H. Zhang, Y. Xing, Preparation of a novel citric acid-crosslinked Zn-MOF/chitosan composite and application in adsorption of chromium (VI) and methyl orange from aqueous solution, Carbohydr. Polym. 258 (2021), 117644.
[85] X. He, K.B. Male, P.N. Nesterenko, D. Brabazon, B. Paull, J.H. Luong, Adsorption and desorption of methylene blue on porous carbon monoliths and nanocrystalline cellulose, ACS Appl. Mater. Interfaces 5 (2013) 8796–8804.
[86] H. Tehubijuluw, R. Subagyo, M.F. Yulita, R.E. Nugraha, Y. Kusumawati, H. Bahruji, A.A. Jalil, H. Hartati, D. Prasetyoko, Utilization of red mud waste into mesoporous ZSM-5 for methylene blue adsorption-desorption studies, Environ. Sci. Pollut. Res. 28 (2021) 37354–37370.

[87] A.F. Hassan, H. Elhadidy, Production of activated carbons from waste carpets and its application in methylene blue adsorption: Kinetic and thermodynamic studies, J. Environ. Chem. Eng. 5 (2017) 955–963.
[88] D. Pathania, S. Sharma, P. Singh, Removal of methylene blue by adsorption onto activated carbon developed from Ficus carica bast, Arab. J. Chem. 10 (2017) S1445–S1451.
[89] L. Li, X.L. Liu, H.Y. Geng, B. Hu, G.W. Song, Z.S. Xu, A MOF/graphite oxide hybrid (MOF: HKUST-1) material for the adsorption of methylene blue from aqueous solution, J. Mater. Chem. A 1 (2013) 10292–10299.
[90] F. Li, J. Liu, W. Liu, Y. Xu, Y. Cao, B. Chen, M. Xu, Preparation of hyper-cross-linked hydroxylated polystyrene for adsorptive removal of methylene blue, RSC Adv. 11 (2021) 25551–25560.
[91] H.M. Gad, A.A. El-Sayed, Activated carbon from agricultural by-products for the removal of Rhodamine-B from aqueous solution, J. Hazard. Mater. 168 (2009) 1070–1081.
[92] M. Sattar, F. Hayeeye, W. Chinpa, O. Sirichote, Preparation and characterization of poly (lactic acid)/activated carbon composite bead via phase inversion method and its use as adsorbent for Rhodamine B in aqueous solution, J. Environ. Chem. Eng. 5 (2017) 3780–3791.
[93] M. Hema, S. Arivoli, Rhodamine B adsorption by activated carbon, Kinetic and equilibrium studies (2009).
[94] G. Yao, S. Li, J. Xu, H. Liu, Dual-responsive graphene oxide/poly (NIPAM-co-AA) hydrogel as an adsorbent for rhodamine B and imidacloprid, J. Chem. Eng. Data 64 (2019) 4054–4065.
[95] T. Zhang, J. Huang, N-vinylimidazole modified hyper-cross-linked resins and their adsorption toward Rhodamine B: Effect of the cross-linking degree, J. Taiwan Inst. Chem. Eng. 80 (2017) 293–300.